Audio Engineering Society

Convention Paper

Presented at the 143rd Convention
2017 October 18–21, New York, NY, USA

Theory of Constant Directivity Circular-Arc Line Arrays

Richard Taylor[1] and D. B. (Don) Keele, Jr.[2]

[1]*Thompson Rivers University, Kamloops BC, Canada*
[2]*DBK Associates and Labs, Bloomington, IN 47408, USA*

Correspondence should be addressed to Richard Taylor (rtaylor@tru.ca)

ABSTRACT

We develop the theory for a broadband constant-beamwidth transducer (CBT) formed by a continuous circular-arc isophase line source. Appropriate amplitude shading of the source distribution leads to a far-field radiation pattern that is constant above a cutoff frequency determined by the prescribed beam width and arc radius. We derive two shading functions, with cosine and Chebyshev polynomial forms, optimized to minimize this cutoff frequency and thereby extend constant-beamwidth behavior over the widest possible band. We illustrate the theory with simulations of magnitude responses, full-sphere radiation patterns and directivity index, for example designs with both wide- and narrow-beam radiation patterns.

1 Introduction

There is considerable interest in the design of acoustic sources with broadband constant directivity, i.e. a radiation pattern that is independent of frequency. Much of this interest stems from work by Toole and others (see [1] and references therein) showing that constant directivity is correlated with subjective perception of quality in stereo reproduction. Constant directivity beamforming also has much broader application to both sensor and transducer arrays for use in audio, broadband sonar, ultrasound imaging, and radar and other remote sensing applications [2, 3, 4].

Keele [5, 6, 7, 8] has reported extensively on a constant-beamwidth transducer (CBT) formed by a circular-arc array of source elements with amplitude shading. Keele's work is based on that of Rogers and Van Buren [2], who showed that a transducer with constant beam pattern can be formed by a spherical cap with frequency-independent amplitude shading based on a Legendre function. Rather fortuitously, when Legendre shading is employed in a circular-arc array a substantially frequency-independent radiation pattern results [6].

Despite the many advantages of circular-arc CBT line arrays, an adequate theory does not appear in the literature. Keele's previous work in this area is empirical. Legendre shading in particular has been given only *post hoc* justification; shading functions adapted to circular arrays have not been developed. While circular arrays are discussed extensively in the literature on electromagnetic antennas (see [9, 10, 11] for a review), there they are widely regarded as narrow-band transducers only. Except in the literature on microphone arrays [12, 13, 14, 15] their potential for broadband constant directivity appears to be unknown.

The aims of the present work are twofold: to establish a theoretical foundation to account for the observed constant directivity behavior of circular-arc arrays, and to derive improved shading functions adapted to these arrays. The paper is structured as follows. In the following section we develop the theory for acoustic radiation from an amplitude-shaded circular arc. We then use this theory to derive conditions on the shading function that guarantee a frequency-independent radiation pattern. On this basis we develop two suitable families of optimal shading functions. Finally, we present results of simulations that illustrate and confirm several key aspects of our theory.

2 Radiation from a Circular Array

Consider a time-harmonic line source in the form of a circle of radius a, in free space, as shown in Fig. 1.

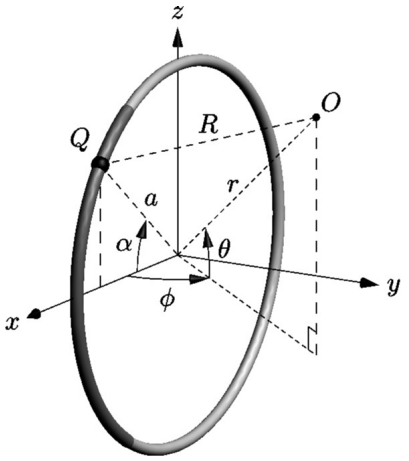

Fig. 1: Circular line source geometry. The shaded arc is the active part of the array considered in the balance of the paper.

We adopt a coordinate system in which the circle is oriented vertically, in the xz-plane, with its center at the origin. We take the x-axis ($\theta = \phi = 0$) to be the primary "on-axis" direction of the resulting radiation pattern. We assume the source distribution is continuous and iso-phase, with amplitude that varies with polar angle α according to a dimensionless and frequency-independent "shading function" $S(\alpha)$ (also sometimes called the amplitude taper or aperture function).

Referring to Fig. 1, the pressure at O due to a unit point source at Q is e^{-ikR}/R (up to a multiplicative constant) where k is the wave number [16, p. 311]. Summing the continuous distribution of point-source contributions around the circle gives the total (complex) pressure p via the Rayleigh integral

$$p(r,\theta,\phi) = \int_0^{2\pi} S(\alpha)\frac{e^{-ikR}}{R}\,d\alpha \qquad (1)$$

where

$$R = \sqrt{a^2 + r^2 - 2ar\cos\phi\cos(\theta-\alpha)}$$
$$\approx r - a\cos\phi\cos(\theta-\alpha) \qquad (r \gg a). \qquad (2)$$

On making the usual far-field ($r \gg a$) approximations and the change of variables $u = \alpha - \theta$, eq. (1) gives

$$p = \frac{e^{-ikr}}{r}\int_0^{2\pi} S(u+\theta)e^{ika\cos\phi\cos u}\,du. \qquad (3)$$

Assuming the shading function $S(\alpha)$ is even, it can then be expressed as a Fourier cosine series

$$S(\alpha) = \sum_{n=0}^{\infty} a_n\cos(n\alpha). \qquad (4)$$

(In the antenna literature on circular arrays, this is called an expansion in "amplitude modes", or circular harmonics, as opposed to the "phase modes" $e^{in\alpha}$ [17].) We refer to each term in eq. (4) as a shading mode. On substitution into eq. (3) this gives

$$p = \frac{e^{-ikr}}{r}\sum_{n=0}^{\infty} a_n f_n(ka\cos\phi)\cos(n\theta) \qquad (5)$$

with the "mode amplitudes" f_n given by

$$f_n(x) = 2\pi i^n J_n(x) \qquad (6)$$

where J_n is a Bessel function of the first kind [18]. Eq. (5) gives the far-field pressure radiated by our circular array.

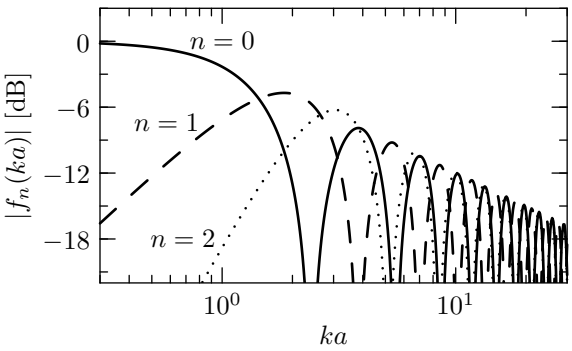

Fig. 2: Mode amplitudes: on-axis far-field pressure, as function of dimensionless frequency ka, for radiation from a circular array with $\cos(n\theta)$ amplitude shading.

Remarks

- Eq. (5) shows that each circular harmonic shading mode gives rise to a far-field radiation mode of the same polar form. The amplitude of each radiation mode is determined by a factor $f_n(ka\cos\phi)$ that depends only on ϕ and the dimensionless frequency ka.
- Therefore, for a full-circle array with single-mode shading $S(\alpha) = \cos(n\alpha)$, the far-field polar pattern in any vertical plane through the origin (constant ϕ) is identical to the shading function at *all* frequencies.
- However, for any single shading mode, destructive interference between opposite sides of the array creates a series of nulls in the frequency response (similar to comb filtering), as illustrated in Fig. 2 which plots the mode amplitudes as a function of frequency. Eqs. (5)–(6) show that these nulls occur when $ka\cos\phi$ coincides with a root of the Bessel function J_n.
- Owing to these response nulls, no full-circle array with single-mode shading can produce a usable

broadband response: at any point in the far field there are frequencies at which the radiated pressure is zero. (This is the "mode stability" problem in the antenna literature [11].)

We can obtain an approximation valid at low frequency by using the asymptotic form [18]

$$J_n(x) \approx \frac{1}{n!}\left(\frac{x}{2}\right)^n \qquad (x \ll 1) \tag{7}$$

in (5) to give

$$p \approx \frac{e^{-ikr}}{r}\sum_{n=0}^{\infty} a_n \cdot \frac{2\pi i^n (ka)^n}{2^n n!}\cos^n\phi\cos(n\theta). \tag{8}$$

From eq. (8) we see that amplitude of the the n^{th} mode falls off at $6n$ dB/oct at low frequency ($ka \to 0$), as Fig. 2 confirms. All shading modes above $n = 0$ radiate very inefficiently at low frequency; the limiting radiation pattern is therefore determined by the first non-zero term in (8). If $a_0 \neq 0$ then the low-frequency radiation pattern is omni-directional: the array radiates like a point source at the origin. If $a_0 = 0$ but $a_1 \neq 0$ then the array exhibits dipole radiation at low frequency.

3 Conditions for Constant Directivity

Here we derive conditions on the shading function $S(\alpha)$ such that the radiation pattern of eq. (5) is independent of frequency. Using the asymptotic form [18]

$$J_n(x) \approx \sqrt{\frac{2}{\pi x}}\cos(x - n\tfrac{\pi}{2} - \tfrac{\pi}{4}) \quad (x \gg n) \tag{9}$$

in (6) gives, after some algebra,

$$f_n(x) \approx \sqrt{\frac{8\pi}{x}}\begin{cases}\cos(x-\frac{\pi}{4}) & n \text{ even}\\ i\sin(x-\frac{\pi}{4}) & n \text{ odd.}\end{cases} \tag{10}$$

Thus, provided $x \equiv ka\cos\phi \gg n$ for all non-negligible terms in (5) we obtain

$$p \approx \frac{e^{-ikr}}{r}\sqrt{\frac{8\pi}{x}}\left[S_e(\theta)\cos(x-\tfrac{\pi}{4}) + iS_o(\theta)\sin(x-\tfrac{\pi}{4})\right] \tag{11}$$

where

$$S_o(\theta) = \sum_{n\,\text{odd}} a_n\cos(n\theta), \tag{12}$$

$$S_e(\theta) = \sum_{n\,\text{even}} a_n\cos(n\theta). \tag{13}$$

Eq. (11) gives the pressure magnitude

$$|p| = \frac{1}{r}\sqrt{\frac{8\pi}{x}}\sqrt{S_e^2(\theta)\cos^2(x-\tfrac{\pi}{4}) + S_o^2(\theta)\sin^2(x-\tfrac{\pi}{4})}. \tag{14}$$

If $|S_e(\theta)| = |S_o(\theta)|$ for all θ then we obtain the far-field pressure

$$|p| = \frac{1}{r}\sqrt{\frac{8\pi}{ka}}\cdot\frac{|S_o(\theta)|}{\sqrt{\cos\phi}}. \tag{15}$$

Critically for our purposes, ***the amplitude of this radiation pattern changes with frequency but its shape does not***.

Thus, the far-field radiation pattern of a circular array will be independent of frequency provided the shading function $S(\alpha)$ satisfies the following conditions:

1. $S = S_o + S_e$ with S_o, S_e given by eqs. (12)–(13) and $|S_o| = |S_e|$.
2. For all non-negligible coefficients a_n in the cosine series for $S(\alpha)$ we have $ka\cos\phi \gg n$.

(These conditions are identical to those given in [3] for the case of radiation from a spherical array, except in that case the a_n are the coefficients of the shading function expanded in spherical harmonics.) Several remarks are in order:

- Condition 1 is equivalent to requiring that, for each θ, at most one of $S(\theta)$ and $S(\pi-\theta)$ is non-zero. In particular this holds if the array is active only on a half-circle on one side of the yz-plane in Fig. 1. In this case one can show that $|S_o(\theta)| = |S(\theta)|/2$, so eq. (15) shows that the limiting beam pattern is *identical to the shading function* in any vertical plane through the origin ($\phi =$ constant).
- Condition 2 ensures a constant beam pattern above a "cutoff frequency" determined by the requirement that $ka\cos\phi \gg n_{\max}$ where $n_{\max}$ is the largest n for which the cosine series coefficient a_n is non-negligible. For greater out-of-plane angles ϕ the cutoff frequency is correspondingly higher.
- Together, these conditions ensure a usable broadband response, without the nulls apparent in Fig. 2. Indeed, for frequencies above cutoff, eq. (15) predicts a smooth dependence of amplitude on frequency everywhere in the far field, with output falling off at 3 dB/oct. (In a practical device this rolloff may require compensatory equalization.)
- To minimize the cutoff frequency (and thereby achieve a constant beam pattern over the widest possible band) we need a shading function whose non-negligible coefficients a_n are of the lowest order possible. In the following section we consider how to design such a function.

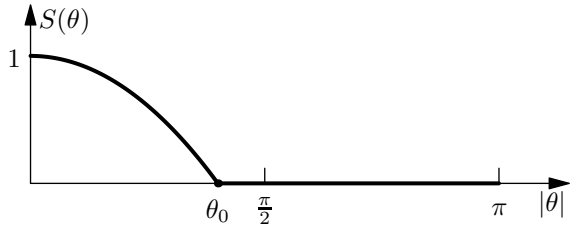

Fig. 3: Shading function restricted to the arc $|\theta| \leq \theta_0$.

- The limiting radiation pattern given by eq. (15) is symmetric across the *yz*-plane, although the array is not. The pattern is unaffected if the array is reflected across this plane.
- Eq. (15) gives a limiting $1/\sqrt{\cos\phi}$ horizontal pattern, hence amplitude peaks along the axis of the circle, as Keele has observed [6]. These peaks are due to the fact that radiation from all elements arrives in-phase at any point on the *y*-axis, whereas in the plane of the array there is some destructive interference among sources. This interference increasing with decreasing wavelength, causing the 3 dB/oct rolloff noted above.

4 Optimal Amplitude Shading

The choice of shading function is critical to achieving broadband constant directivity from a circular-arc array. A good shading function must have its Fourier spectrum concentrated in its lowest-order terms, and be non-zero only on a circular arc $|\theta| \leq \theta_0 \leq \frac{\pi}{2}$. The general form of such a shading function is shown in Fig. 3.

Legendre shading, developed for spherical arrays in [2], has been used extensively by Keele in his work on CBT arrays [5, 6, 7, 8]. Since Legendre functions serve to minimize the amplitude of higher-order terms when the shading function is expanded in spherical harmonics [2], which are themselves polynomials in $\cos\theta$, we can see why Legendre shading behaves well when employed on a circular arc. However, being adapted to a spherical rather than circular radiator, Legendre shading might not be the optimal choice. In the appendices we develop two new shading functions, with the goal of constant beam-width radiation over the widest possible band.

Appendix A shows that the cosine shading

$$S(\theta) = \begin{cases} \cos\left(\frac{\pi}{2} \cdot \frac{\theta}{\theta_0}\right) & |\theta| \leq \theta_0 \\ 0 & \theta_0 < |\theta| \leq \pi \end{cases} \tag{16}$$

is optimal in the sense that its cosine series coefficients $|a_n|$ are at a local minimum (as a function of θ_0) for all $n \gtrsim \pi/(2\theta_0)$.

Remarks

- The cosine shading (16) is analogous to (but much simpler than) the Legendre function $P_\nu(\cos\theta)$ developed in [2]; the two are identical in the case $\theta_0 = \frac{\pi}{2}$.
- The parameter θ_0 controls the beam width of the array. The design equations for cosine shading are particularly simple: we have $\theta_0 = \frac{3}{2}\theta_6$ where θ_6 is the desired -6 dB half-angle in the plane of the array. By contrast, the design equations for Legendre shading cannot be expressed in closed form, and require numerical root-finding as well as evaluation of the rather obscure Legendre functions.
- Decreasing θ_0 (i.e. narrowing the beam width) increases the index $n_{\max}$ above which the cosine series coefficients a_n are minimized. Since the cutoff frequency is determined by the condition $ka\cos\phi \gg n_{\max}$, we see that (for a given arc radius) a narrower beam leads to a higher cutoff frequency.

Appendix B shows that the Chebyshev polynomial shading

$$S(\theta) = \begin{cases} T_N\left(2 \cdot \frac{1+\cos\theta}{1+\cos\theta_0} - 1\right) & |\theta| \leq \theta_0 \\ 0 & \theta_0 < |\theta| \leq \pi, \end{cases} \tag{17}$$

where T_N is the Nth Chebyshev polynomial, is optimal in the sense that it is very close to a degree-N polynomial in $\cos\theta$. Together, the parameters N and θ_0 control the beam width and arc coverage. For a given angle θ_0, increasing N results in a narrower beam. As we illustrate below, this shading function is in many ways superior to both cosine and the Legendre function shading used in [5].

5 Examples

To confirm and illustrate the key aspects of our theoretical results above, here we present simulations of two particular circular-arc arrays designed to achieve broadband constant directivity, but with different beam widths. One is a wide-beam array with the cosine shading

$$S(\theta) = \begin{cases} \cos\left(\frac{9}{7}\theta\right) & |\theta| \leq 70^\circ \\ 0 & |\theta| > 70^\circ \end{cases} \tag{18}$$

which gives a -6 dB half-angle of 47°. The other is a narrow-beam array with the degree-6 Chebyshev polynomial shading

$$S(\theta) = \begin{cases} T_6\left(2 \cdot \frac{1+\cos\theta}{1+\cos 52^\circ} - 1\right) & |\theta| \leq 52^\circ \\ 0 & |\theta| > 52^\circ \end{cases} \tag{19}$$

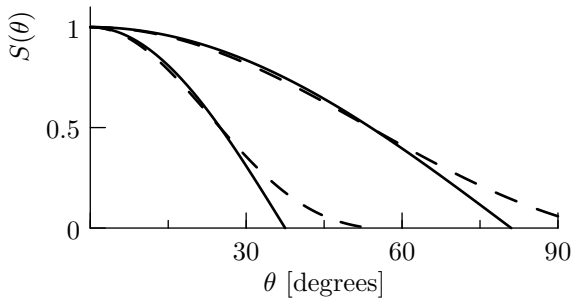

Fig. 4: Shading functions with -6 dB beam half-angles of 25° and 47°, via cosine shading [solid] and Chebyshev shading [dashed]. The degree-6 Chebyshev polynomial (19) was used for the narrow beam; a degree-2 polynomial was used for the wider beam.

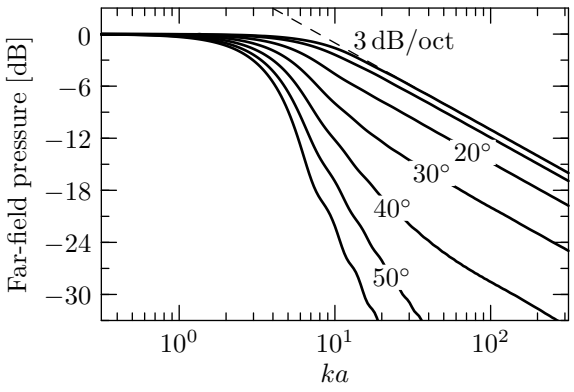

Fig. 5: Far-field (unequalized) magnitude response at various angles θ in the plane of an array with the Chebyshev shading (19).

which gives a -6 dB half-angle of 25°.

The shading functions in eqs. (18)–(19) are plotted in Fig. 4, together with other shading functions that achieve the same beam widths. Chebyshev shading, especially with higher polynomial degree, gives a more gradual taper near the end of the arc. This results in smoother frequency response (see Fig. 7 below) at the expense of requiring greater arc coverage for a given beam width.

5.1 Magnitude Response

Fig. 5 shows the raw (unequalized) far-field magnitude responses at various angles θ in the plane of an array ($\phi = 0$) with the narrow-beam shading of eq. (19). These were calculated by numerical quadrature (via an adaptive Simpson's rule) of the Rayleigh integral in eq. (3). The responses are plotted against the dimensionless frequency ka. (For reference, an array of radius $a = 1$ m has $ka = 1$ at 54 Hz.)

Fig. 5 confirms several aspects of the theory developed above. There is a clear cutoff frequency ($ka \approx 10$) above which the radiation pattern transitions from omnidirectional to a frequency-independent pattern determined by the shading function. Above cutoff the level rolls off at 3 dB/oct at all off-axis angles, as predicted by eq. (15). In marked contrast with a full-circle array (Fig. 2), the shaded circular-arc array provides a usable response at all frequencies, without nulls or significant ripples.

For both the wide-beam cosine shading (18) and narrow-beam Chebyshev shading (19), Fig. 6 shows the far-field magnitude responses at various angles θ in the plane of the array, this time normalized to the on-axis ($\theta = 0$) response. In agreement with our theory, above the cutoff frequency ($ka \approx 2$ for the wide-beam example; $ka \approx 20$ for the narrow-beam case) the normalized response becomes constant at all angles, indicating a constant beam pattern.

To illustrate the benefits of Chebyshev versus Legendre function shading, Fig. 7 shows the far-field magnitude response at various angles in the plane of the array, for two arrays shaded to achieve a -6 dB beam half-angle of 25°: one with Legendre function shading as in [5], the other with the degree-6 Chebyshev shading of eq. (19). The Legendre-shaded array exhibits response ripples of several dB, while the Chebyshev-shaded array has a ripple-free response at all off-axis angles. Moreover, with increasing frequency the Chebyshev-shaded arrays settles more quickly into a frequency-independent radiation pattern, particularly at angles beyond 30°.

5.2 Full-Sphere Radiation Patterns

For the two shading functions considered above, Fig. 8 shows the full 3D radiation patterns (polar balloons), calculated at several frequencies via numerical quadrature of the integral in eq. (3), and normalized to the on-axis response. As expected, in both cases there is a transition from monopole radiation at low frequency to a frequency-independent radiation pattern above the cutoff frequency. Above cutoff the full radiation pattern is remarkably constant in both cases, except near the y-axis where the pattern settles down only at the highest frequencies. In agreement with eq. (15), the limiting vertical pattern is determined by the shading function, while the horizontal pattern has a broad $1/\sqrt{\cos\phi}$ shape with corresponding amplitude peaks on the y-axes. At all frequencies the radiation patterns are symmetric front-to-back (i.e. across the yz-plane).

5.3 Directivity Index

The directivity index [19] characterizes the directivity of a radiation pattern $p(r, \theta, \phi)$ in terms of the ratio of

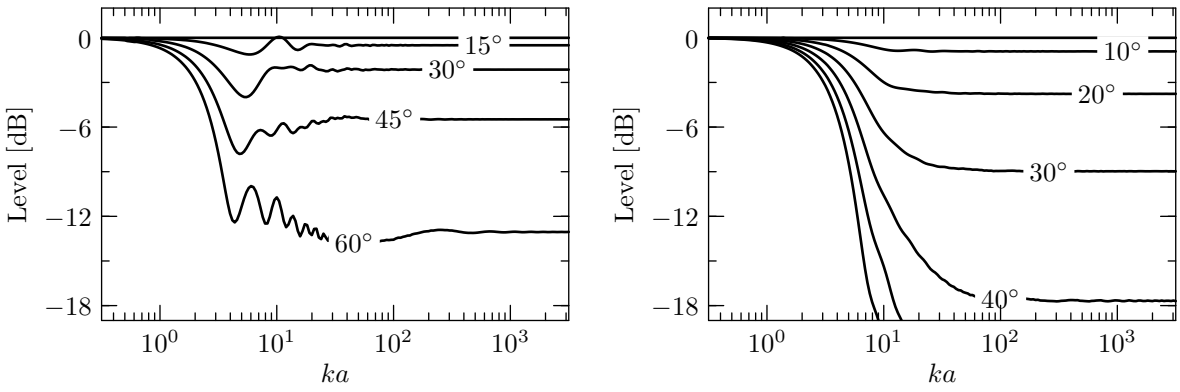

(a) Wide Beam **(b)** Narrow Beam

Fig. 6: Far-field magnitude responses at various angles θ in the plane of the array, normalized to the on-axis ($\theta = 0$) response, for **(a)** a wide-beam array with the cosine shading of eq. (18), and **(b)** a narrow-beam array with the Chebyshev shading of eq. (19).

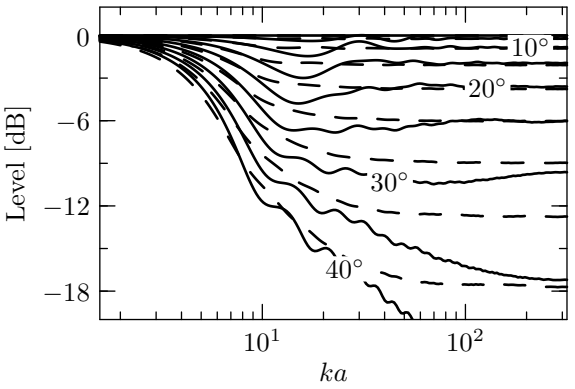

Fig. 7: Far-field magnitude responses at various angles θ in the plane of the array, normalized to the on-axis ($\theta = 0$) response, for arrays with -6 dB beam half-angle of 25° via Legendre function shading [solid] and the Chebyshev shading (19) [dashed].

the on-axis intensity to that of a point source radiating the same total power. For the coordinate system of Fig. 1 the directivity index is given by

$$\mathrm{DI} = 10\log_{10}\frac{4\pi|p(r,0,0)|^2}{\int_0^{2\pi}\int_{-\pi/2}^{\pi/2}|p(r,\theta,\phi)|^2\cos\phi\,d\phi\,d\theta}. \tag{20}$$

For both our wide- and narrow-beam examples, Figure 9 shows the directivity index as a function of dimensionless frequency ka, calculated by numerical quadrature of (20) with the radiation pattern given by eq. (3). As expected, both arrays exhibit 0 dB directivity (monopole radiation) at low frequency, with increasing directivity in a transition band around the cutoff frequency of the array, above which the directivity is constant and determined by the array shading. For the wide-beam array in particular the directivity index is remarkably constant, varying by less then 3 dB over all frequencies.

6 Discrete Arrays

Our theory to this point is based on an idealized continuous circular source distribution. However, a practical implementation will involve a finite number of conventional drivers, with strengths determined by sampling the continuous shading function. (Keele [5, 6, 7, 8] has reported experimental results of using various sampling procedures.) This will cause deviations from the theoretical behavior, due to sampling of the shading function, as well as directionality of the sources.

A complete treatment of these effects is beyond the scope of this paper. However, from the relevant theory developed in [10, 11] we can draw some practical conclusions. For a discrete circular array of equally-spaced point sources, for all wavelengths greater than twice

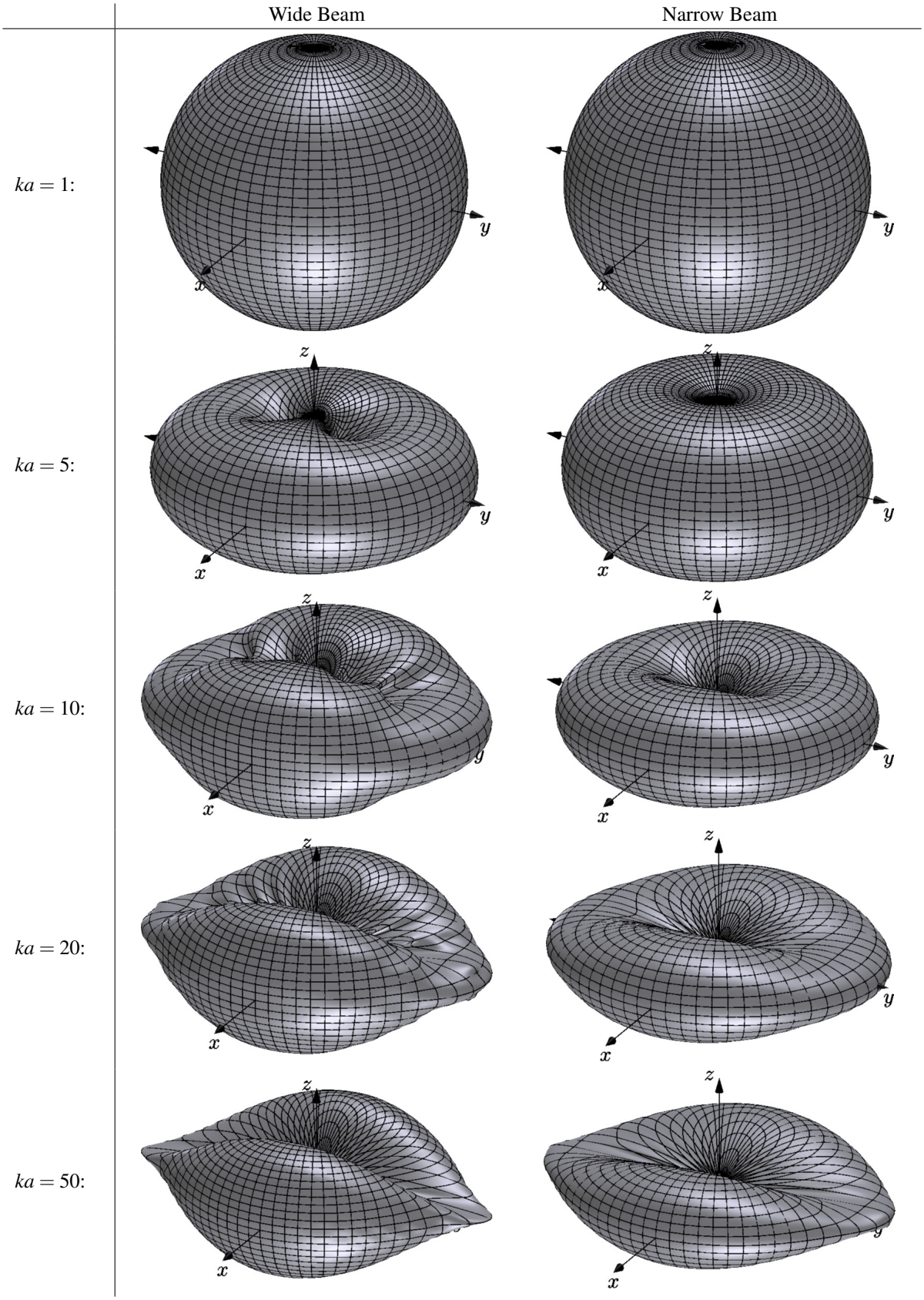

Fig. 8: 3D radiation patterns (polar balloons) for circular-arc arrays with the wide-beam cosine shading of eq. (18) and narrow-beam Chebyshev shading of eq. (19). The array is oriented as shown in Fig. 1. All plots are normalized on-axis.

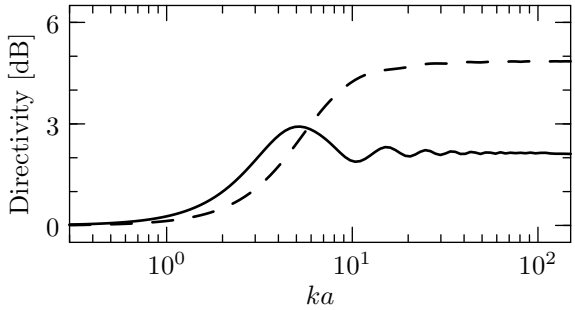

Fig. 9: Directivity index for arrays with the wide-beam cosine shading of eq. (18) [solid] and narrow-beam Chebyshev shading of eq. (19) [dashed].

the source spacing, errors introduced by sampling the shading function are insignificant, provided there are at least two point sources per spatial period corresponding to the highest-order non-negligible term in the cosine series (4) (this result is analogous to the Nyquist sampling theorem). When the source spacing exceeds a half-wavelength, spatial aliasing (due to destructive interference between finitely-spaced sources) causes a highly irregular response, and the discrete array is a poor approximation of the continuous ideal. In practical terms, this means the example arrays considered here can be well-approximated by discrete arrays of as few as 10 point sources, up to the frequency where spatial aliasing ensues.

The effect of physical sources' departure from ideal point-source behavior is more difficult to treat, particularly since for circular arrays there is no simple theory analogous to the product theorem for *linear* arrays of directional sources. For circular arrays, the mathematical treatment of directional elements is covered in [10, 11]. Its effects on our theory of constant directivity circular-arc arrays will be the subject of future work.

7 Conclusion

We have developed a theory that accounts for the observed [5, 6, 7, 8] constant directivity behavior of amplitude-shaded circular-arc line arrays. The key to understanding and optimizing such arrays is to express the shading function (amplitude taper) in terms of an expansion in circular harmonics (cosine series). The conclusions that follow are remarkably parallel to those for an amplitude-shaded spherical cap, as developed in [2, 3]:

- The radiation pattern becomes asymptotically frequency-independent above a cutoff frequency determined by the arc radius and the order of the highest-order non-negligible term in the shading function's cosine series. The cutoff frequency is inversely proportional to the arc radius and prescribed beam width.

- Above cutoff the constant radiation pattern is a product of a vertical pattern (i.e. in the plane of the array) that agrees with the shading function, and a horizontal pattern that has a broad $1/\sqrt{\cos\phi}$ form that gives a high amplitude peak within a small solid angle around the axis of the circular arc. Above cutoff the frequency response rolls off at 3 dB/oct.

- Below cutoff, directivity control is lost: the radiation pattern becomes omni-directional, with constant frequency response.

These theoretical results are corroborated by Keele's earlier measurements and simulations [6, 7], as well as the simulations presented here.

Our theory indicates how to design the amplitude shading so as to achieve constant directivity over the widest band possible: the Fourier spectrum of the shading function must be concentrated in its lowest-order terms. This explains Keele's observations that shading with a Legendre function (borrowed from [2]) behaves very well, but it also opens the way to designing better shading functions. Here we have developed two new shading functions adapted to circular-arc arrays: one based on a simple cosine form, the other based on Chebyshev polynomials. Cosine shading has the advantage of being quite simple, and allows for the widest beam pattern. Chebyshev polynomial shading gives a better-controlled frequency response, at the expense of requiring greater arc coverage for a given beam width.

Practical implementation of our theory is beyond the scope of this paper. Several engineering issues arise, including spatial aliasing due to finite (rather than continuous) spacing of sources, departure of source elements from ideal point-source behavior, mutual coupling between source elements, and physical implementation of the shading function via a resistive network. Many of these issues have been addressed at length by Keele elsewhere [7, 8].

A major benefit of CBT spherical-cap arrays, shown theoretically in [2], is that *both* the near- and far-field radiation pattern agree with the shading function, and thus there is no essential difference between the near- and far-field behaviors. Unfortunately the (far-field) theory presented here does not account for this important aspect of circular-arc line arrays; we plan to address this issue in future work.

References

[1] Toole, F., *Sound Reproduction: The Acoustics and Psychoacoustics of Loudspeakers and Rooms*, Focal Press, 2008.

[2] Rogers, P. H. and Van Buren, A. L., "New approach to a constant beamwidth transducer," *Journal of the Acoustical Society of America*, 64(1), pp. 38–43, 1978.

[3] Jarzynski, J. and Trott, W. J., "Array shading for a broadband constant directivity transducer," *Journal of the Acoustical Society of America*, 64(5), pp. 1266–1269, 1978.

[4] Ward, D. B., Kennedy, R. A., and Williamson, R. C., "Constant Directivity Beamforming," in M. Brandstein and D. Ward, editors, *Microphone Arrays: Signal Processing Techniques and Applications*, chapter 1, Springer, 2013.

[5] Keele, Jr., D. B., "The application of broadband constant beamwidth transducer (CBT) theory to loudspeaker arrays," in *Audio Engineering Society Convention 109*, Audio Engineering Society, 2000.

[6] Keele, Jr., D. B., "The full-sphere sound field of constant beamwidth transducer (CBT) loudspeaker line arrays," in *Audio Engineering Society Convention 114*, Audio Engineering Society, 2003.

[7] Keele, Jr., D. B., "Practical implementation of constant beamwidth transducer (CBT) loudspeaker circular-arc line arrays," in *Audio Engineering Society Convention 115*, Audio Engineering Society, 2003.

[8] Keele, Jr., D. B. and Button, D. J., "Groundplane constant beamwidth transducer (CBT) loudspeaker circular-arc line arrays," in *Audio Engineering Society Convention 119*, Audio Engineering Society, 2005.

[9] Hansen, R. C., *Phased Array Antennas*, Wiley, 2009.

[10] Mailloux, R. J., *Phased Array Antenna Handbook*, Artech House (Boston), 2005.

[11] Josefsson, L. and Persson, P., *Conformal Array Antenna Theory and Design*, Wiley, 2006.

[12] Yong Wang, Yixin Wang, Yuanling Ma, Zhengyao He, and YuKang Liu, "Broadband pattern synthesis for circular sensor arrays," *Journal of the Acoustical Society of America*, 136(2), pp. EL153–158, 2014.

[13] Mu PengCheng, Yin QinYe, and Zhang JianGuo, "A wideband beamforming method based on directional uniform circular arrays," *Science China Information Sciences*, 53(12), pp. 2600–2609, 2010.

[14] Parthy, A., Epain, N., van Schaik, A., and Jin, C. T., "Comparison of the measured and theoretical performance of a broadband circular microphone array," *Journal of the Acoustical Society of America*, 130(6), pp. 3827–3837, 2011.

[15] Meyer, J., "Beamforming for a circular microphone array mounted on spherically shaped objects," *Journal of the Acoustical Society of America*, 109, pp. 185–193, 2001.

[16] Morse, P. M. and Ingard, K. U., *Theoretical Acoustics*, Princeton University Press, 1987.

[17] Davies, D. E. N., "Circular Arrays," in A. W. Rudge, K. Milne, A. D. Olver, and P. Knight, editors, *The handbook of antenna design*, volume 2, chapter 12, Peter Peregrinus, 1983.

[18] DLMF, "*NIST Digital Library of Mathematical Functions*," http://dlmf.nist.gov/, Release 1.0.13, 2016, F. W. J. Olver, A. B. Olde Daalhuis, D. W. Lozier, B. I. Schneider, R. F. Boisvert, C. W. Clark, B. R. Miller and B. V. Saunders, eds.

[19] Beranek, L. L. and Mellow, T. J., *Acoustics: Sound Fields and Transducers*, Academic Press, 2012.

[20] Carothers, N. L., "A short course on approximation theory," `http://personal.bgsu.edu/~carother/Notes/ApproxTheorySu09-Final.pdf`, 1998, Bowling Green State University, Bowling Green, OH [Online; accessed 31-May-2017].

Appendix A. Cosine Shading

To derive an optimal shading for circular-arc arrays, here we adapt the technique that was used in [2] to derive Legendre function shading for a spherical cap. We seek an even shading function

$$S(\theta) = \begin{cases} f(\theta) & |\theta| \le \theta_0 \\ 0 & \theta_0 < |\theta| \le \pi \end{cases} \tag{21}$$

where the arc half-angle $\theta_0 \le \frac{\pi}{2}$ is given and f is a function to be determined. From eq. (4) the cosine series coefficients are then

$$a_n = \frac{2}{\pi} \int_0^{\theta_0} f(\theta) \cos(n\theta)\, d\theta \qquad (n > 0). \tag{22}$$

To concentrate the shading function's Fourier spectrum in its lowest-order terms, our strategy is to determine

f so that a_n^2 is minimized (as a function of θ_0) for all $n > N$, while the a_n^2 are maximized for $n \le N$.

Making all the a_n stationary with respect to θ_0 requires that

$$0 = \frac{da_n}{d\theta_0} = \frac{2}{\pi} \cdot f(\theta_0)\cos(n\theta_0). \tag{23}$$

Satisfying this equation for all n requires $f(\theta_0) = 0$, i.e. f should have a root at the arc endpoint θ_0. We take this to be the *smallest* such root, since the beam pattern would otherwise have undesirable side-lobes. We can then assume without loss of generality that $f(\theta) > 0$ for $0 < \theta < \theta_0$.

To distinguish whether the a_n^2 are maximized or minimized as a function of θ_0 we employ the second derivative test; to this end we evaluate

$$\frac{d^2a_n^2}{d\theta_0^2} = \frac{4}{\pi} a_n f'(\theta_0)\cos(n\theta_0). \tag{24}$$

Let N be the integer such that for all $n \le N$ the smallest root of $\cos(n\theta)$ is greater than θ_0, while for $n > N'$ the smallest root is less than θ_0. Thus,

$$N = \lfloor \pi/(2\theta_0) \rfloor \tag{25}$$

where $\lfloor \cdot \rfloor$ denotes the integer part. Then for $n \le N$ we have $\cos(n\theta) > 0$ on $[0, \theta_0]$, hence $a_n > 0$ by eq. (22). Assuming $f'(\theta_0) < 0$ gives $d^2a_n^2/d\theta_0^2 < 0$, so that each of the a_n^2 ($n \le N$) is indeed a local *maximum* as a function of θ_0.

Now we need to ensure that a_n^2 is a local *minimum* as a function of θ_0 for all $n > N$, which would require $d^2a_n^2/d\theta_0^2 > 0$. Thus, from eq. (24) we require

$$\cos(n\theta_0) \int_0^{\theta_0} f(\theta)\cos(n\theta)\, d\theta < 0 \quad (n > N). \tag{26}$$

This gives the shading function

$$f(\theta) = \cos\left(\tfrac{\pi}{2} \cdot \tfrac{\theta}{\theta_0}\right). \tag{27}$$

as one possible choice that satisfies (26) together with our various other assumptions. Indeed, we have

$$\begin{aligned} &\cos(n\theta_0) \int_0^{\theta_0} f(\theta)\cos(n\theta)\, d\theta \\ &\qquad = \frac{\left(\frac{\pi}{2\theta_0}\right)^2}{\left(\frac{\pi}{2\theta_0}\right)^2 - n^2} \cdot \cos^2(n\theta_0) < 0 \end{aligned} \tag{28}$$

when $n > N = \lfloor \pi/(2\theta_0) \rfloor$ so that (26) is satisfied and a_n^2 is indeed a local minimum, as a function of θ_0, for all $n > N$. Thus the cosine function (27) is (in one particular sense) an optimal choice of shading function.

Appendix B. Chebyshev Shading

Here we take a different (and in many ways better) approach to optimally shading a circular-arc array to achieve broadband constant directivity. Again we seek a shading function $S(\theta)$ of the form (21). We employ the following strategy to obtain a function whose cosine series is concentrated in the lowest-order terms: we let $f(\theta)$ be a low-order polynomial in $\cos\theta$, chosen so that $f(\theta)$ vanishes, as nearly as possible, throughout the interval $[\theta_0, \pi]$. When we form $S(\theta)$ by truncating $f(\theta)$ to zero on this interval, as in (21), its cosine series coefficients a_n will change very little, and so will remain concentrated in the lowest orders.

To this end, let $S(\theta)$ be given by (21) where

$$f(\theta) = P(\cos\theta) \tag{29}$$

and P is a polynomial of degree N. We want the maximum of $|P(x)|$ to be as small as possible for $x \in [-1, x_0]$ where $x_0 = \cos\theta_0$. This criterion uniquely determines that $P(x)$ is a Chebyshev polynomial [20]. (Alternatively we could seek to minimize $P(x)$ in the least-squares sense, in which case P is a Legendre polynomial. This gives a shading function that is only slightly different.)

The first few Chebyshev polynomials $T_N(u)$ are given, up to a multiplicative constant, by

$$\begin{aligned} T_1(u) &= u & T_3(u) &= 4u^3 - 3u \\ T_2(u) &= u^2 - 1 & T_4(u) &= 8u^4 - 8u^2 + 1. \end{aligned} \tag{30}$$

Each T_N is the monic polynomial of degree N whose maximum absolute value on $[-1, 1]$ is a minimum [20, p. 36]. Moreover, each $|T_N(u)|$ maximizes its values (relative to this minimum) outside the interval $[-1, 1]$.

To obtain the polynomial $P(x)$ that vanishes as nearly as possible on $[-1, x_0]$ we form $P(u(x))$ where $u(x)$ is a linear function that takes $x \in [-1, x_0]$ to $u \in [-1, 1]$ [20, p. 37]. This gives the shading function

$$f(\theta) = P\big(u(\cos\theta)\big) = T_N\left(2 \cdot \frac{1 + \cos\theta}{1 + \cos\theta_0} - 1\right). \tag{31}$$